

Electronic Supplementary Information (ESI) for the manuscript:

**pH-Switching of the luminescent, redox, and magnetic properties in a spin
crossover cobalt(II) molecular nanomagnet**

Renato Rabelo, Luminita Toma, Nicolás Moliner, Miguel Julve, Francesc Lloret, Mario Inclán, Enrique García-España, Jorge Pasán,

Rafael Ruiz-García and Joan Cano*

TABLE OF CONTENTS

Materials	S3
Preparation of the ligands	S3
Methyl 4'-(4-carboxyphenyl)-2,2'/6',2''-terpyridine (MeL)	
4'-(4-carboxyphenyl)-2,2'/6',2''-terpyridine (HL)	
Sodium 4'-(4-carboxylatephenyl)-2,2'/6',2''-terpyridine (NaL)	
Scheme S1	
Preparation of the complexes	S5
$\{[\text{Co}(\text{HL})_2][\text{Co}(\text{HL})\text{L}]\}(\text{ClO}_4)_3 \cdot 9\text{H}_2\text{O}$ (1)	
$[\text{CoL}_2] \cdot 5\text{H}_2\text{O}$ (2)	
Scheme S2	
Physical techniques	S7
Physicochemical characterisation	S8
Fig. S1 – S3	
X-ray crystallographic data collection and structure refinement	S10
Table S1 and S2	
Fig. S4 – S9	
EPR spectra	S17
Fig. S10	
Static and dynamic magnetic measurements	S18
Fig. S11 – S16	
Solution studies	S24
Fig. S17 – S19	

Materials

Reagent grade 2-acetylpyridine, methyl 4-formylbenzoate, sodium hydroxide, ammonium acetate, cobalt(II) acetate tetrahydrate, cobalt(II) perchlorate hexahydrate, and polyethyleneglycol-200 were purchased from commercial sources and used as received.

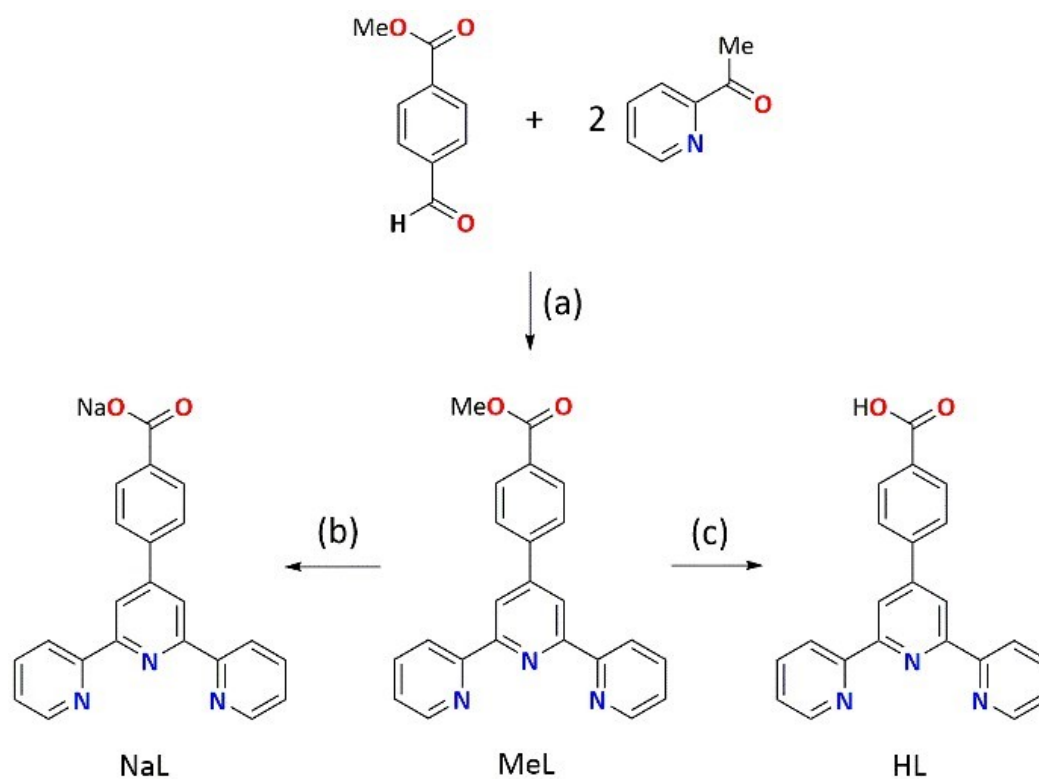
Preparation of the ligands

Methyl 4'-(4-carboxyphenyl)-2,2':6',2''-terpyridine (MeL): 2-Acetylpyridine (3.10 mL, 27.5 mmol) was added to PEG200 (40 mL) containing NaOH (1.10 g, 27.5 mmol), and the resulting suspension was stirred for 15 minutes at 0 °C. Later, methyl 4-formylbenzoate (2.25 g, 13.75 mmol) was added and the whole was kept at 0 °C for two hours under vigorous stirring. Then, an excess of ammonium acetate (6.70 g, 87.0 mmol) was added to the reaction mixture and further heated at 100 °C for two hours. The reaction mixture was cooled to room temperature, and 200 mL of water was added to cause the precipitation of the yellow crude methyl ester acid product (MeL). The yellow solid was collected by filtration and washed with water and cold ethanol. Yield ca 42%. Anal. Calc. for C₂₃H₁₇N₃O₂ (MeL): C, 75.19; H, 4.66; N, 11.44. Found: C, 74.67; H, 4.34; N, 11.20%. IR (KBr, cm⁻¹): 1706s, and 1288s [$\nu(\text{COO})_{\text{as}}$, and $\nu(\text{COO})_{\text{s}}$, respectively, from methoxycarbonyl group]; 2950w [$\nu(\text{C}_{\text{sp}3}-\text{H})$ from the methyl substituents]; 1579s and 767s [$\nu(\text{C}=\text{N})$ and out-of-plane $\delta(\text{C}_{\text{sp}2}-\text{H})$ from the pyridyl rings]. ¹H NMR (DMSO; 300 MHz, ppm): δ = 9.16-8.84 (m, 3H), 8.42 (d, 1H, J = 6.3 Hz), 8.19 (q, 2H, J = 8.4 Hz), 7.93 (s, 1H).

4'-(4-carboxyphenyl)-2,2':6',2''-terpyridine (HL): The hydrolysis of the methyl ester acid derivative was carried out under basic medium by treating MeL (0.30 g, 0.80 mmol) with a 2.0 M NaOH aqueous solution (25 mL) overnight at 100 °C. After cooling at room temperature, the pH of the suspension was adjusted to 3.0 with 3.0 M HCl solution. The white precipitate which formed was filtered and washed several times with water. Yield 95%. Anal. Calc. for C₂₂H₁₅N₃O₂ (HL): C, 74.78; H, 4.28; N, 11.89. Found: C, 74.43; H, 4.25; N, 11.94%. IR (KBr, cm⁻¹): 3417m, 1706s, and 1261s [$\nu(\text{O}-\text{H})$, $\nu(\text{COO})_{\text{as}}$, and $\nu(\text{COO})_{\text{s}}$, respectively, from carboxyl group]; 1595s and 771s [$\nu(\text{C}=\text{N})$ and out-of-plane $\delta(\text{C}_{\text{sp}2}-\text{H})$ from the pyridyl rings]. ¹H NMR (DMSO; 300 MHz, ppm): δ = 9.16-8.84 (m, 3H), 8.42 (d, 1H, J = 6.3 Hz), 8.19 (q, 2H, J = 8.4 Hz), 7.93 (s, 1H).

Sodium 4'-(4-carboxylatephenyl)-2,2':6',2''-terpyridine tetrahydrate (NaL): The hydrolysis of the methyl ester acid derivative was carried out on basic medium by treating MeL (0.50 g, 0.80 mmol) with a 2.0 M NaOH aqueous solution (15 mL) overnight at 100 °C. Yield 64%. Anal. Calc. for C₂₂H₂₂N₃O₆Na (NaL): C, 59.06; H, 4.96; N, 9.39. Found: C, 60.33; H, 4.70; N, 9.14%. IR (KBr, cm⁻¹): 3421-2800 [$\nu(\text{O}-\text{H})$ from crystallisation water], 1562s, and 1402s [$\nu(\text{COO})_{\text{as}}$, and $\nu(\text{COO})_{\text{s}}$ from carboxylate group]; 1602s and 775s [$\nu(\text{C}=\text{N})$ and out-of-plane $\delta(\text{C}_{\text{sp}2}-\text{H})$ from the pyridyl rings]. ¹H NMR (CDCl₃; 300 MHz, ppm): δ = 8.70 (s, 2H, H_{im}), 8.24 (d, 2H, $m\text{-H}_{\text{py}}$, J =

7.8 Hz), 7.90 (t, 1H, p -H_{py}, $J = 7.8$ Hz), 7.36 (d, 4H, o -H_{ph}, $J = 8.9$ Hz), 6.96 (d, 4H, m -H_{ph}, $J = 8.9$ Hz), 3.85 (s, 6H, p -H_{OMe}).

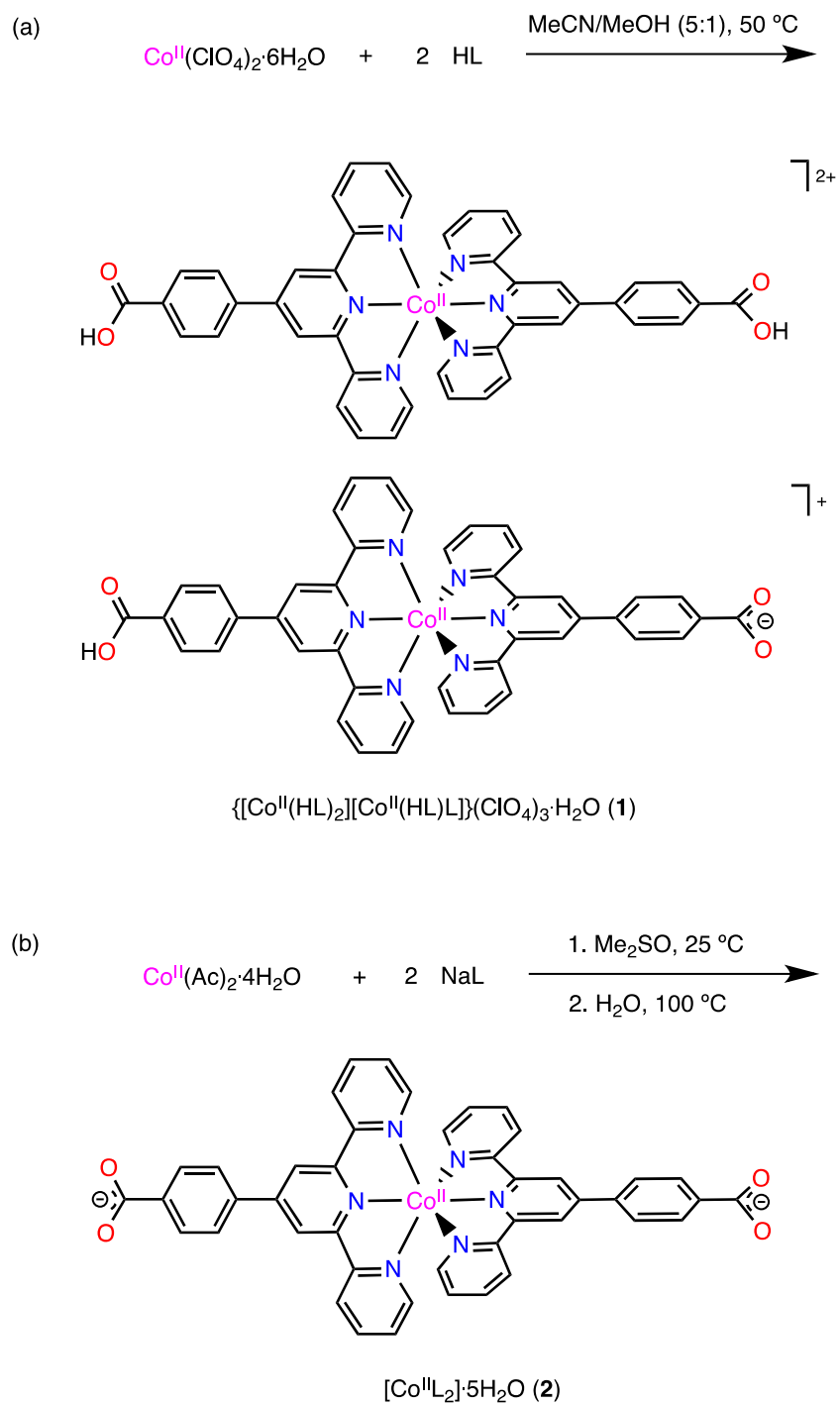


Scheme S1 General synthetic procedure for the preparation of the deprotonated form of the ligand as a sodium salt (NaL) and its protonated acid (HL) from the methyl ester precursor (MeL). Reaction conditions: (a) NaOH (PEG200, 0 °C) and NH₄OAc (100 °C); (b) NaOH (H₂O, 100 °C); (c) HCl (H₂O, 25 °C).

Preparation of the complexes

$\{[Co^{II}(HL)_2][Co^{II}(HL)L]\}(ClO_4)_3 \cdot 9H_2O$ (**1**): A methanolic solution (3.0 mL) of cobalt(II) perchlorate hexahydrate (0.018 g, 0.05 mmol) was added dropwise to a suspension of HL (0.0354 g, 0.10 mmol) in acetonitrile (15.0 mL) under stirring. The mixture was stirred for one hour under gentle warming at 50 °C. The resulting red solution was allowed to evaporate in a hood slowly, and X-ray quality dark red crystals of **1** were obtained after one week. The crystals were collected on filter paper and gently washed with acetonitrile. Yield 72 %. Anal. Calc. for $C_{41}H_{35}N_6O_{12}Cl_2Co$ (**1**): C, 53.18; H, 4.04; N, 8.86. Found: C, 53.98; H, 4.17; N, 8.90%. IR (KBr, cm^{-1}): 3439s [$\nu(O-H)$ from carboxyl group and crystallisation waters], 1689s and 1263s [$\nu(COO)_{as}$, and $\nu(COO)_s$ from carboxyl/carboxylate groups]; 1614 and 775s [$\nu(C=N)$ and out-of-plane $\delta(C_{sp^2}-H)$ from the pyridyl rings]; and 1110vs [$\nu(Cl-O)$ from perchlorate anions].

$[Co^{II}L_2] \cdot 5H_2O$ (**2**): An aqueous solution (15 mL) of cobalt(II) acetate tetrahydrate (0.025 g, 0.10 mmol) was added dropwise to a suspension of NaL (0.075 g, 0.20 mmol) in dimethylsulfoxide (5.0 mL) under stirring. The mixture was stirred for one hour at room temperature. The polycrystalline powder was filtered and washed with a small quantity of water. X-ray quality dark red crystals of **2** were obtained by treating the polycrystalline powder under hydrothermal conditions at 100 °C for four days. Yield 91 %. Anal. Calc. for $C_{44}H_{38}N_6O_9Co$ (**2**): C, 61.90; H, 4.49; N, 9.84. Found: C, 61.75; H, 4.32; N, 9.90%. IR (KBr, cm^{-1}): 3407s [$\nu(O-H)$ from crystallisation waters], 1554s and 1371s [$\nu(COO)_{as}$, and $\nu(COO)_s$ from carboxylate group], and 1553s and 785s [$\nu(C=N)$ and out-of-plane $\delta(C_{sp^2}-H)$ from the pyridyl rings].



Scheme S2 General synthetic procedure for the preparation of **1** (a) and **2** (b).

Physical techniques

Elemental (C, H, N) and energy dispersive X-ray (EDX) analyses were performed at the Servicio Central de Soporte a la Investigación (SCSIE) at the Universitat de València (Spain). FT-IR spectra were recorded on a Nicolet-5700 spectrophotometer as KBr pellets. ^1H NMR spectra were registered at room temperature on a Bruker AC 300 (300 MHz) spectrometer. Deuterated dimethylsulfoxide (DMSO-d_6) was used as solvent and internal standard ($\delta = 2.5$ ppm). Powder X-ray diffraction (PXRD) patterns of powdered crystalline samples were collected at room temperature on a D8 Avance A25 Bruker diffractometer using graphite-monochromated $\text{Cu-K}\alpha$ radiation ($\lambda = 1.54056 \text{ \AA}$). Q-band EPR spectra of **1** and **2** as crushed crystals were recorded at 4.0 K under non-saturating conditions in a Bruker ER 200 D spectrometer equipped with a helium-flow cryostat. Variable-temperature (2–300 K) direct current (dc) magnetic susceptibility measurements under applied fields 0.25 ($T < 20$ K) and 5.0 kOe ($T > 20$ K) and variable-field (0–50 kOe) magnetisation measurements at $T = 2.0$ K were carried out on crushed crystals of **1** and **2** with a Quantum Design SQUID magnetometer. The magnetic susceptibility data were corrected for the diamagnetism of the constituent atoms and the sample holder. Variable-temperature (2–300 K) alternating current (ac) magnetic susceptibility measurements under ± 5.0 Oe oscillating field at frequencies in the range 0.1–10 kHz were carried out under different dc magnetic fields ($H_{\text{dc}} = 1.0, 2.5, 3.5$ and 5.0 kOe) with a Quantum Design Physical Property Measurement System (PPMS).

Physicochemical characterisation

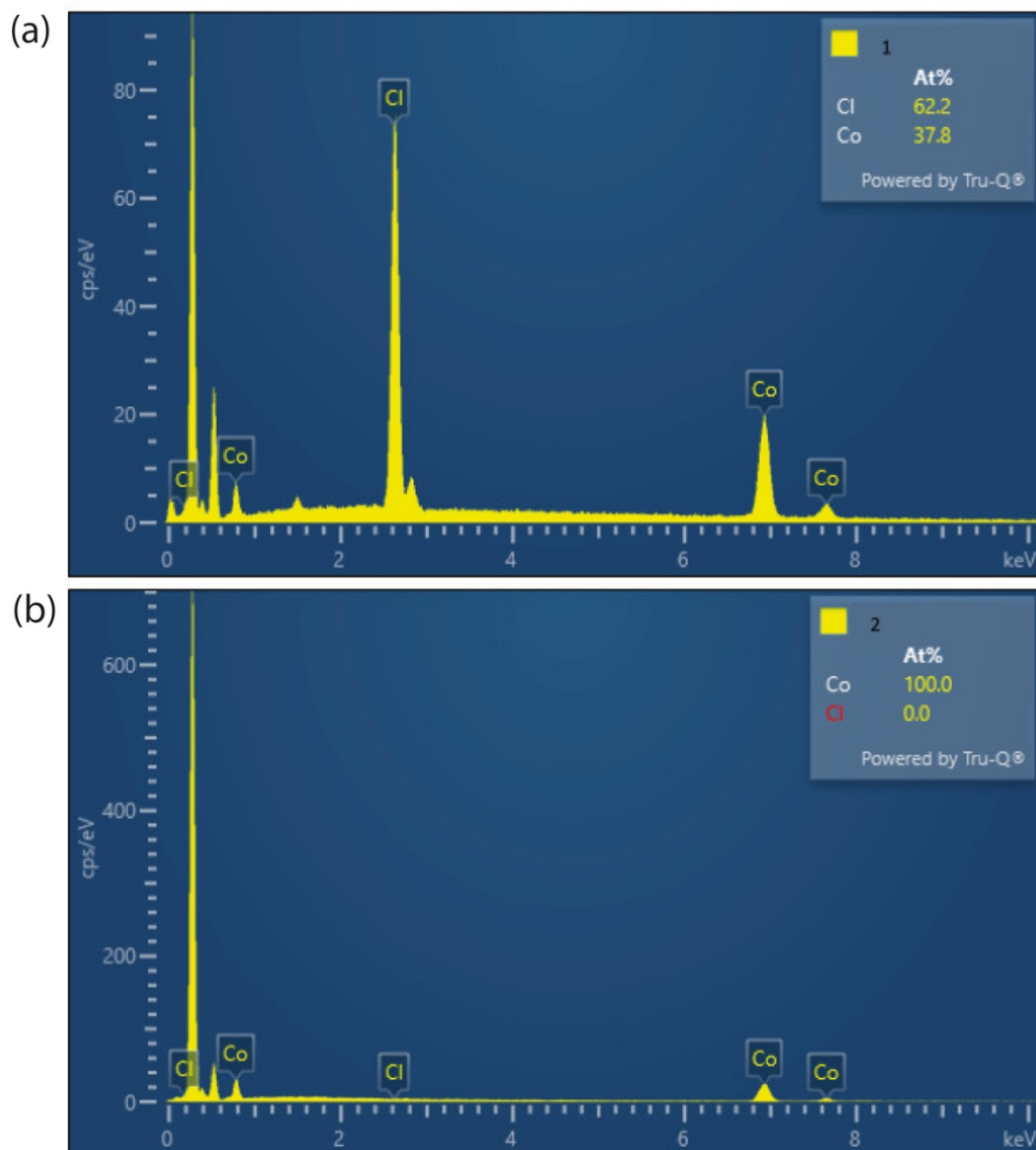


Fig. S1 EDX spectra of **1** (a) and **2** (b). The peaks corresponding to chlorine and cobalt atoms have been labelled to facilitate identification. The insets display the relative atomic percentages of chlorine and cobalt.

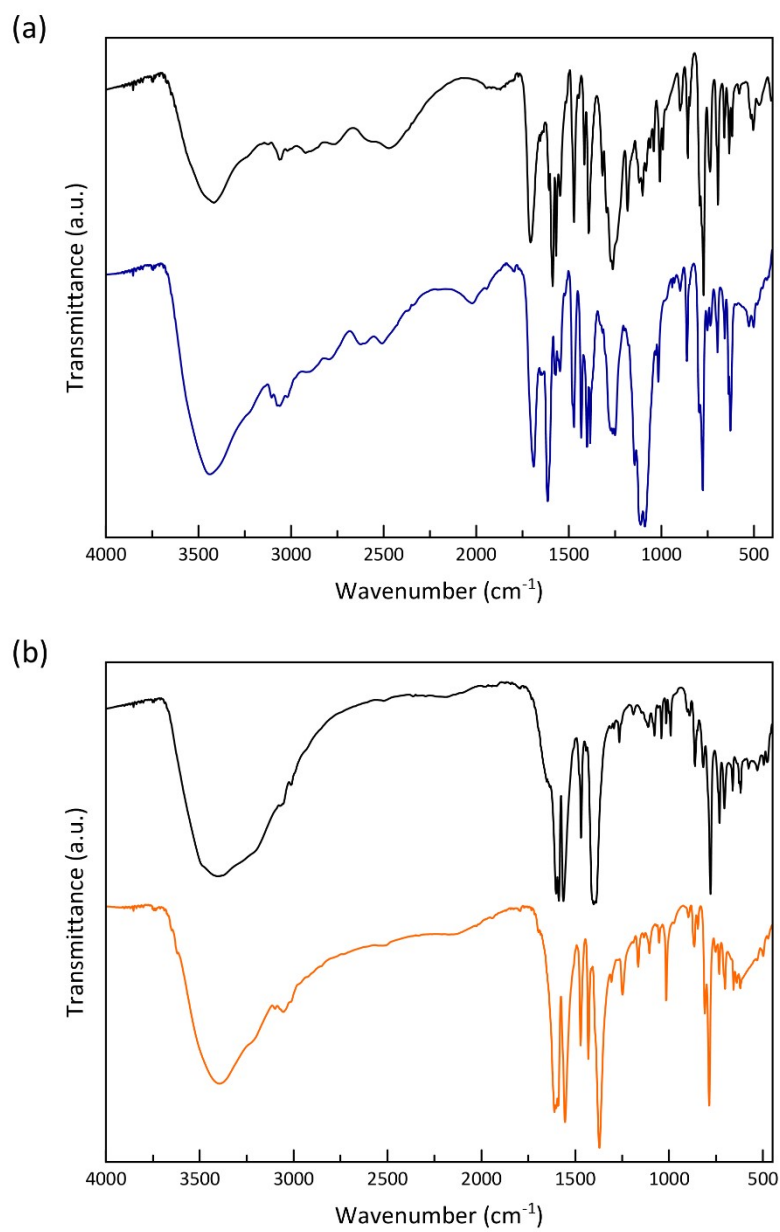


Fig. S2 FT-IR spectra of **1** (blue, a) and **2** (orange, b) compared to those of HL and NaL, respectively (black).

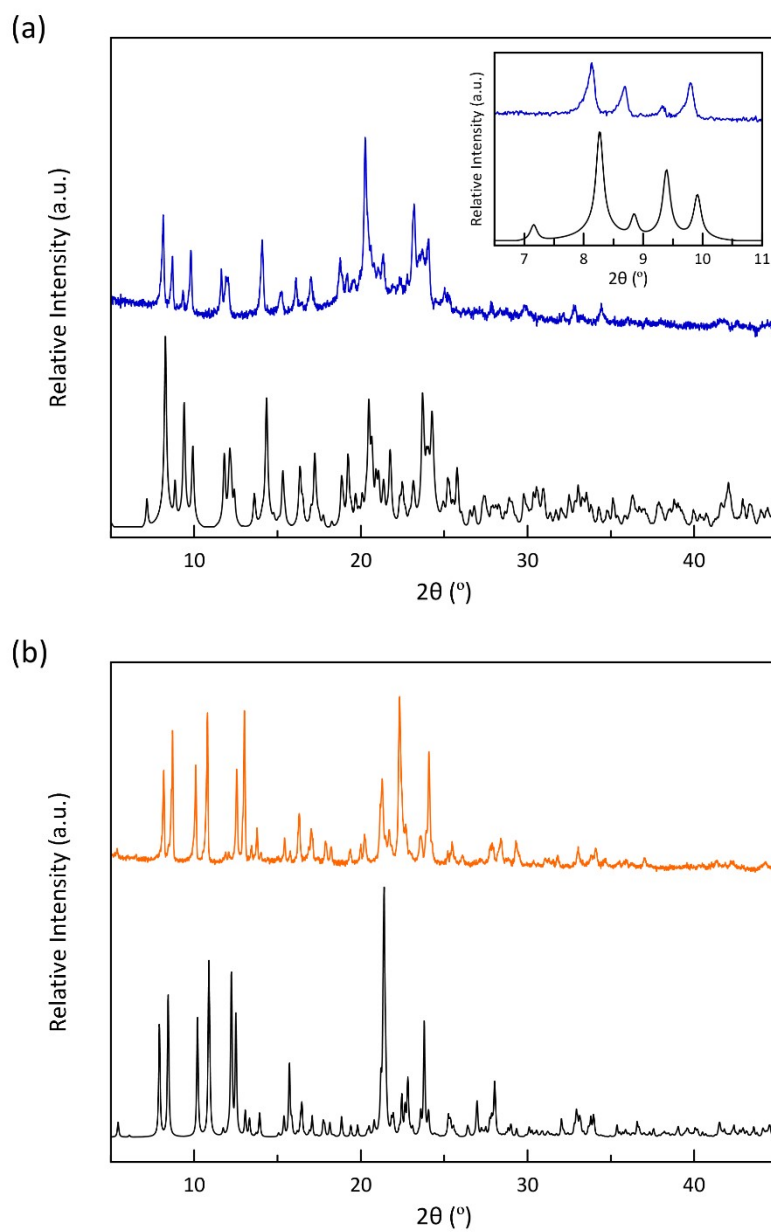


Fig. S3 Experimental PXRD pattern of **1** (blue, a) and **2** (orange, b) compared to the calculated ones (black).

X-ray crystallographic data collection and structure refinement

X-ray diffraction data on a single crystal of **1** and **2** were collected on a Bruker D8 Venture diffractometer with a PHOTON II detector by using monochromatic Mo-K α radiation ($\lambda = 0.71073 \text{ \AA}$) at 120 K. Diffraction data of **1** and **2** were collected, scaled, and integrated using the Bruker SAINT software.¹ The structures were solved by intrinsic phasing methods integrated into the SHELXTL² software with the Olex2 platform.³ The obtained models were refined with the version 2018/3 of SHELXL against F^2 on all data by full-matrix least squares. The diffraction of the single crystal of **2** was somewhat poor, with a low average $I/2\sigma(I)$ and a rather large R_{int} (0.1745). All non-hydrogen atoms were refined anisotropically, except those of one disordered perchlorate anion in the structure of **1** because the refinement, even constrained, was unstable. Hydrogen atoms in water molecules were neither found nor fixed. The remaining ones were set on geometrical positions and refined with a riding model. Hydrogens from carboxyl groups in **1** were set in the longest C–O bond [C22–O2: 1.310(5) \AA vs. C22–O1: 1.203(5) \AA and C44–O4: 1.294(7) \AA vs. C44–O3: 1.216(7) \AA], with an unrefined site occupancy factor of 0.75. The two perchlorate anions in **1** were disordered and constraints (EADP), and soft and rigid restraints (SADI or DFIX) were used to refine the disorder in a model accounting for two positions. The somewhat high residual electron density corresponds to disordered solvent around the water molecules O16 and O17. Further modelling of the disorder creates a messy refinement model. The low residual electron density was not squeezed with a mask to avoid the inclusion of artifacts. In the crystal structure of **2**, some occupation factors for water molecules (O6, O7, O8 and O10) were refined and later fixed to the closest round value (s.o.f. set at 0.5). The O11 and O12 water molecules were refined with the s.o.f. values linked, leading to values also close to 0.5. The graphical manipulations and calculations were performed with the CRYSTALMAKER and MERCURY programs.^{4,5}

Crystallographic data (excluding structure factors) for the structures reported in this paper have been deposited with the Cambridge Crystallographic Data Centre as supplementary publication numbers CCDC–2230369 (**1**) and 2230370 (**2**). Copies of the data can be obtained free of charge from the Cambridge Crystallographic Data Centre via www.ccdc.cam.ac.uk/structures.

¹ Bruker. *SAINT*. Bruker AXS Inc., Madison, Wisconsin, USA, **2012**.

² Sheldrick, G. M. SHELXT - Integrated Space-Group and Crystal-Structure Determination. *Acta Cryst.* **2015**, *A71*, 3–8.

³ Dolomanov, O.V., Bourhis, L.J., Gildea, R.J., Howard, J.A.K. & Puschmann, H. J. OLEX2: A Complete Structure Solution, Refinement and Analysis Program. *Appl. Cryst.* **2009**, *42*, 339–341.

⁴ *CrystalMaker*, CrystalMaker Software, Bicester, England, **2015**.

⁵ *Mercury*, The Cambridge Crystallographic Data Centre, Cambridge, UK.

Table S1 Summary of Crystallographic Data for **1** and **2**

	1	2
Formula	C ₈₈ H ₇₆ N ₁₂ O _{28.5} Cl ₃ Co ₂	C ₄₄ H ₃₈ N ₆ O ₉ Co
<i>M</i> (g mol ⁻¹)	1981.83	853.65
Crystal system	Triclinic	Triclinic
Space group	<i>P</i> -1	<i>P</i> -1
<i>a</i> (Å)	9.224(4)	8.7247(5)
<i>b</i> (Å)	12.380(5)	13.4869(7)
<i>c</i> (Å)	19.363(7)	16.4323(8)
α (°)	85.759(15)	93.298(2)
β (°)	77.184(15)	97.277(2)
γ (°)	89.430(15)	91.254(2)
<i>V</i> (Å ³)	2150.0(14)	1913.99(18)
<i>Z</i>	1	2
ρ_{calc} (g cm ⁻³)	1.517	1.481
μ (mm ⁻¹)	0.570	0.517
<i>T</i> (K)	120	120
Reflect. collected	46691	100316
Reflect. obs. [<i>I</i> > 2 σ (<i>I</i>)]	7617 (6578)	23465 (9769)
Data/restraints/parameters	7614/59/668	23465/0/569
<i>R</i> ₁ ^a [<i>I</i> > 2 σ (<i>I</i>)] / <i>R</i> ₁ (all)	0.0704 / 0.0790	0.0987 / 0.2509
<i>wR</i> ₂ ^b [<i>I</i> > 2 σ (<i>I</i>)] / <i>wR</i> ₂ (all)	0.2028 / 0.2120	0.1599 / 0.2183
<i>S</i> ^c	1.056	1.013

^a $R_1 = \sum(|F_o| - |F_c|) / \sum|F_o|$. ^b $wR_2 = [\sum w(F_o^2 - F_c^2)^2 / \sum w(F_o^2)^2]^{1/2}$. ^c $S = [\sum w(|F_o| - |F_c|)^2 / (N_o - N_p)]^{1/2}$.

Table S2 Selected Structural Data for **1** and **2**

	1 (<i>T</i> = 120 K)	2 (<i>T</i> = 120 K)	2 (<i>T</i> = 153 K) ⁶
$R_1(\text{Co}-\text{N}_p)^a$ (Å)	2.081(4)	2.030(2)	2.158(2)
$R_2(\text{Co}-\text{N}'_p)^a$ (Å)	2.049(4)	2.113(2)	2.134(2)
$R_3(\text{Co}-\text{N}_c)^b$ (Å)	1.894(4)	1.897(2)	1.896(2)
R_{eq}^c (Å)	2.065(4)	2.071(2)	2.146(2)
R^d (Å)	2.008(4)	2.013(2)	2.063(2)
Δ_R^e	0.085(4)	0.086(2)	0.121(2)
δ_R^f	0.017(4)	0.040(2)	0.011(2)
$\text{N}_p-\text{Co}-\text{N}'_p^g$ (°)	94.664(15)	92.25(8)	94.40(8)
$\text{N}'_p-\text{Co}-\text{N}_p^g$ (°)	89.13(15)	91.35(8)	88.94(8)
$\text{N}_c-\text{Co}-\text{N}_c^h$ (°)	179.74(16)	176.46(9)	176.53(9)
δ^i (Å)	±0.358(4)	±0.368(2)	±0.367(2)
Φ^j (°)	83.57(3)	89.65(2)	87.42(2)
φ^k (°)	7.08(8)/43.62(11)	14.30(5)/29.57(6)	27.54(7)/19.32(11)
$d_1(\text{C}=\text{O})^l$ (Å)	1.203(6)/1.216(7)	1.258(4)	1.306 (4)
$d_2(\text{C}-\text{O})^l$ (Å)	1.310(5)/1.294(7)	-	-
Δ_{CO}^m (Å)	0.107(7)/0.078(7)	-	-

^aAverage equatorial bond lengths from each ligand. ^bAverage axial bond lengths. ^cAverage equatorial bond lengths defined as $R_{\text{eq}} = (R_1 + R_2)/2$. ^dAverage cobalt-nitrogen bond lengths defined as $R = (R_1 + R_2 + R_3)/3$. ^eAxial distortion parameter defined as $\Delta_R = (R_{\text{eq}} - R_3)/R$. ^fRhombic distortion parameter defined as $\delta_R = (R_1 - R_2)/R_{\text{eq}}$. ^gAverage equatorial bond angles. ^hAverage axial bond angles. ⁱAverage deviations of the distal pyridyl-nitrogen donor atoms from the mean metal equatorial plane. ^jDihedral angle between the mean planes of the terpyridine ligand fragments. ^kDihedral angle between the mean planes of the terpyridyl and the benzoic/benzoate fragments. ^lCarbon-oxygen bond lengths of each ligand. ^mDifference between the carbon-oxygen bond lengths from the carboxyl/carboxylate groups of each ligand defined as $\Delta_{\text{CO}} = (d_2 - d_1)$.

⁶ J. Yang, R.-X. Hu, M.-B. Zhang, *J. Solid State Chem.*, 2012, **196**, 398–403.

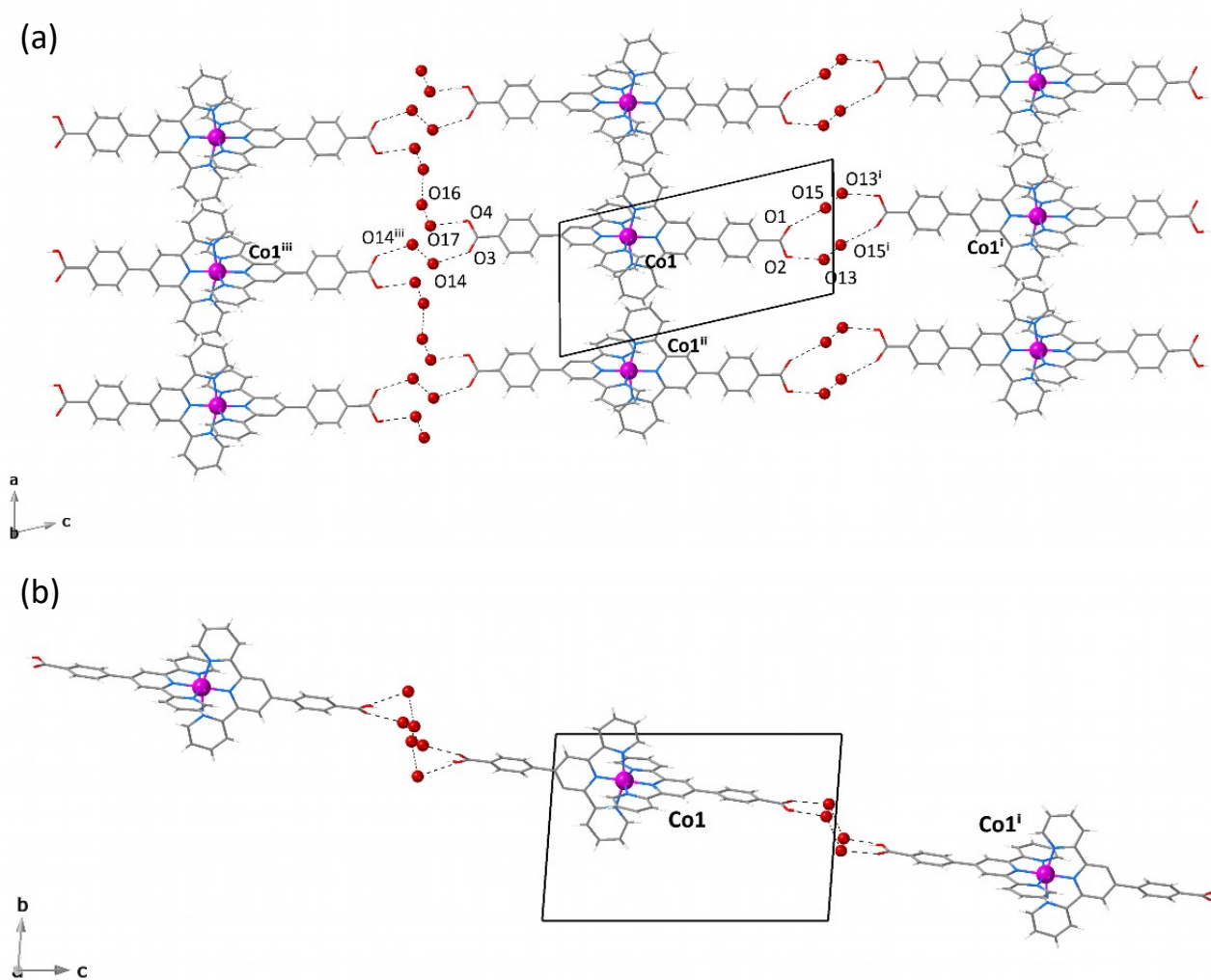


Fig. S4 Views of a single layer of hydrogen-bonded cationic mononuclear cobalt(II) units of **1** along the crystallographic *a* (a) and *c* axes (b) with the atom numbering scheme for the hydrogen-bonded network of perchlorate anions and crystallisation waters [symmetry codes: (i) = $-x, -y, -z$; (ii) = $-x, -y, -z - 1$; (iii) = $-x, -y, 3 - z$]. The hydrogen bonding interactions involving the perchlorate anions and the crystallisation waters are drawn as dotted lines.

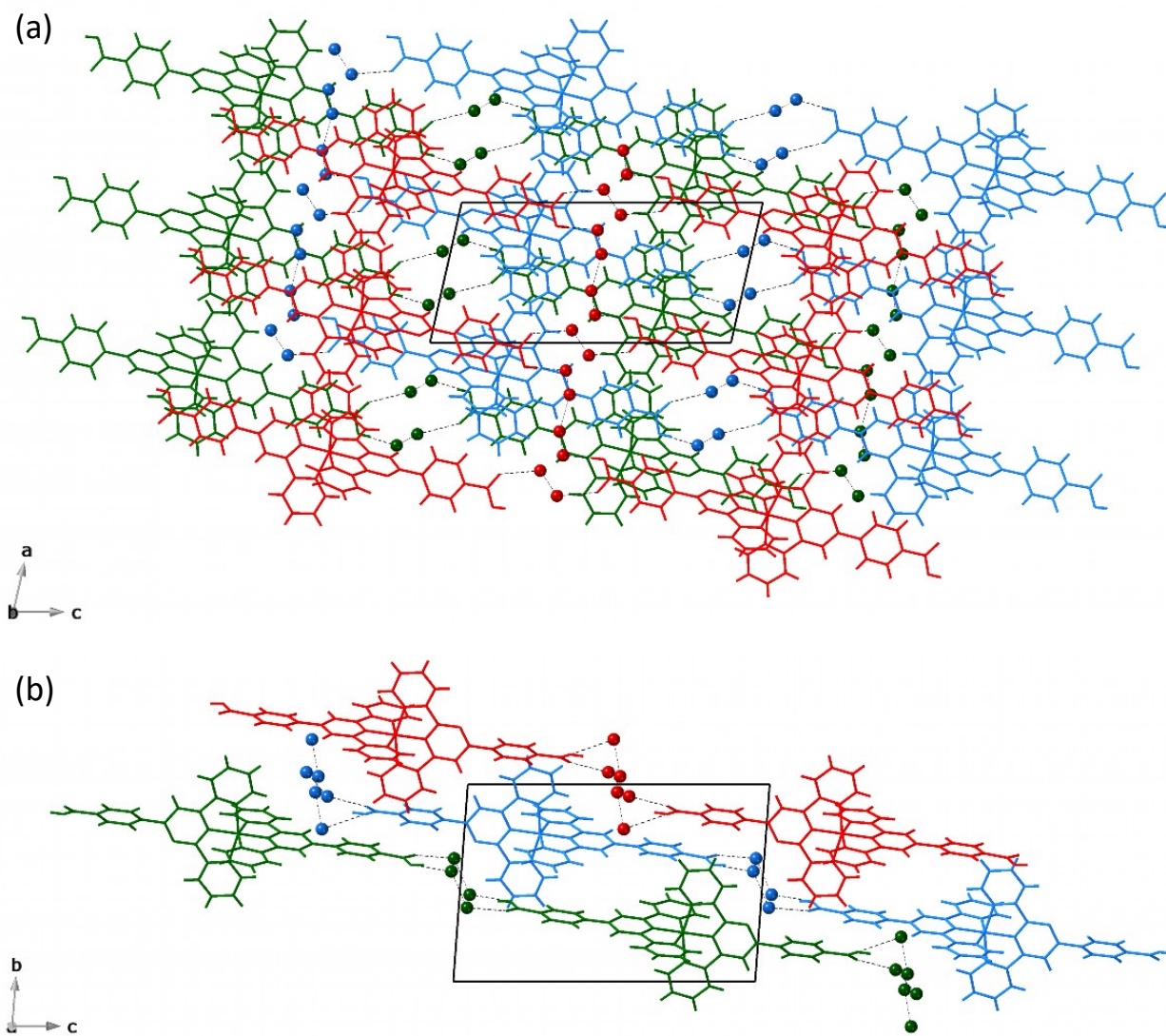


Fig. S5 Perspective views of the crystal packing of **1** along the *b* (a) and *a* axes (b) showing the occupation with the crystallisation waters of the small channels built by the parallel array of cationic mononuclear cobalt(II) units.

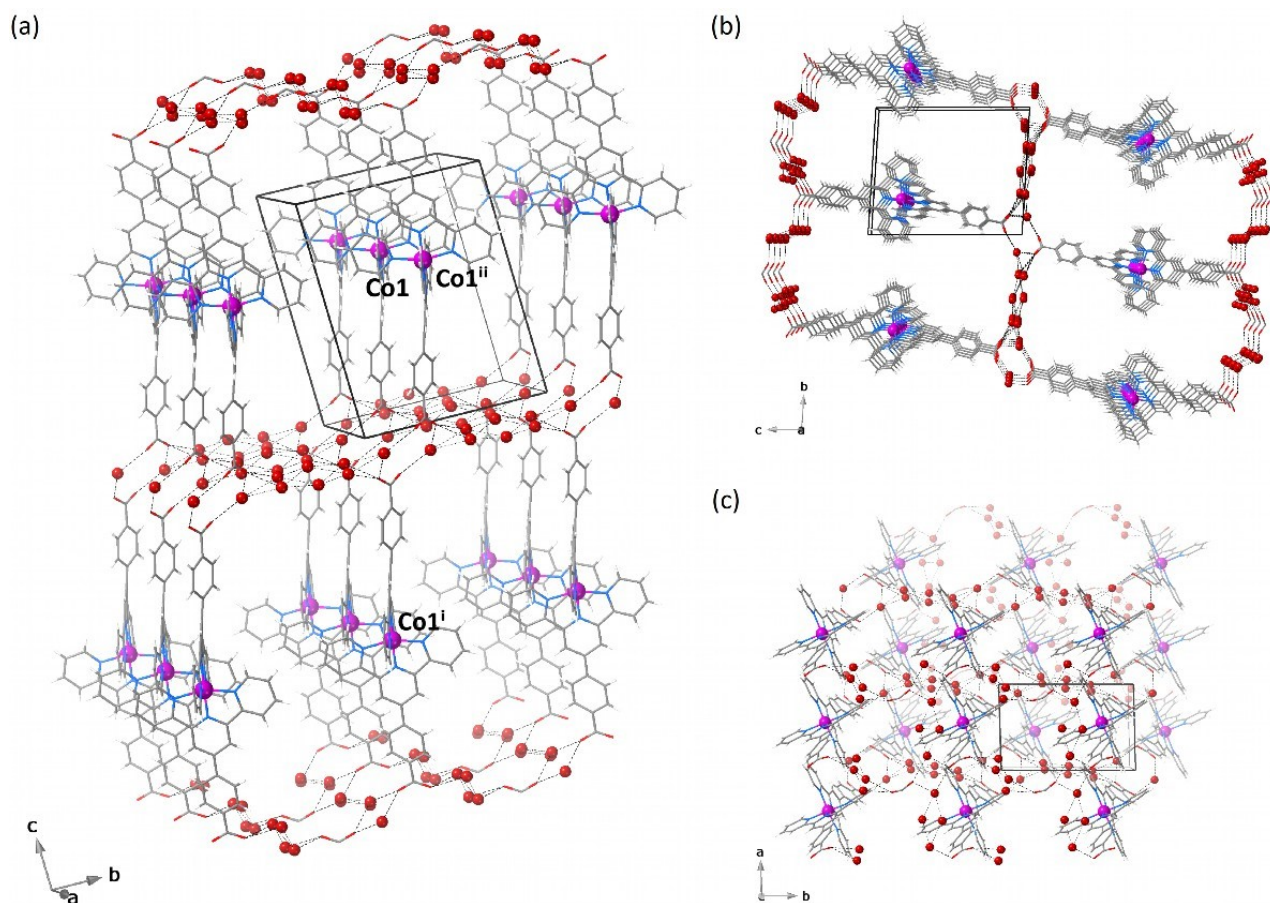


Fig. S6 (a) View of a single pillared layer 3D array of hydrogen-bonded neutral mononuclear cobalt(II) units of **2** with the atom numbering scheme for the hydrogen-bonded network of crystallisation waters [symmetry codes: (i) = $-x, -y, -z$; (ii) = $-x, -y, -z - 1$]. (b) and (c) Perspective views of a hydrogen-bonded pillared layer 3D array along the crystallographic *a* and *c* axes, respectively. The hydrogen bonding interactions involving the free waters are drawn as dotted lines.

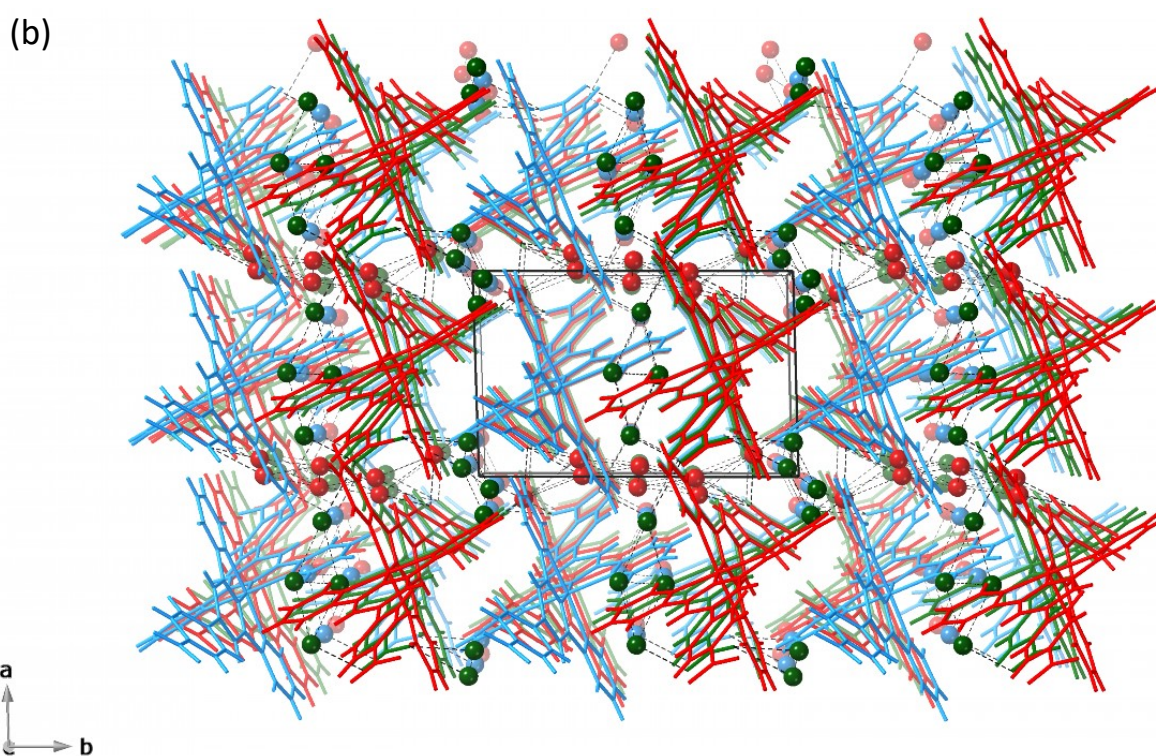
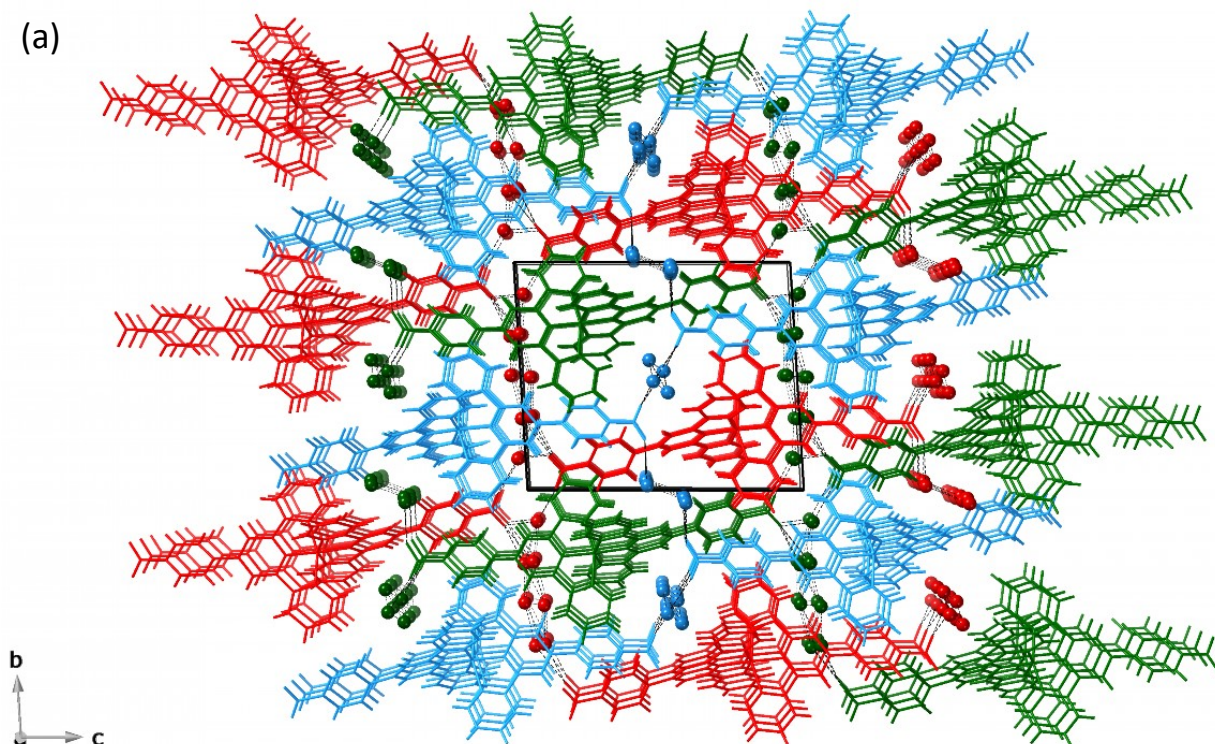


Fig. S7 Projection views of the triply interpenetrated 3D array of hydrogen-bonded neutral mononuclear cobalt(II) units of **2** along the crystallographic *a* and *c* axes (a and b, respectively). The hydrogen bonding interactions with the crystallisation waters are drawn as dotted lines.

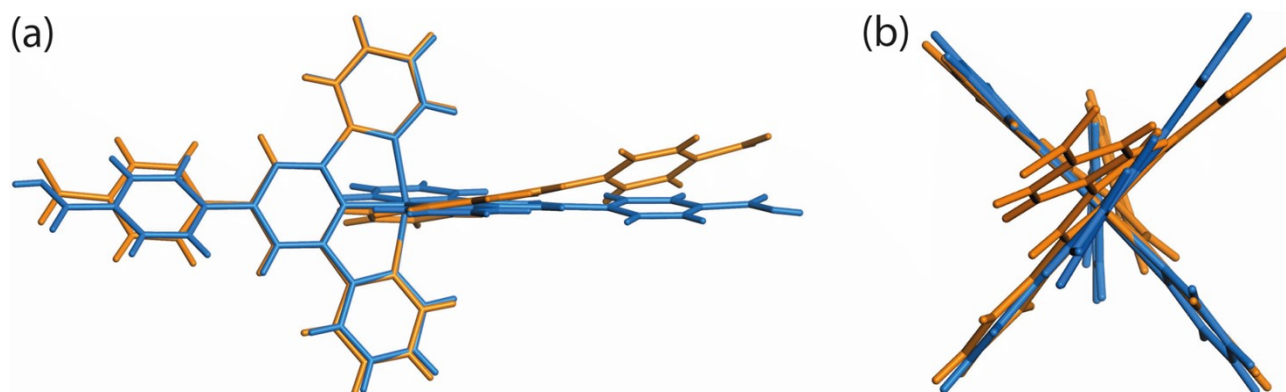


Fig. S8 (a) Front and (b) side superposition views of the cationic equivalent protonated/hemiprotonated (blue) and neutral deprotonated (orange) mononuclear cobalt(II) units of **1** and **2**. The ligand backbones are shown in green and red colours, respectively.

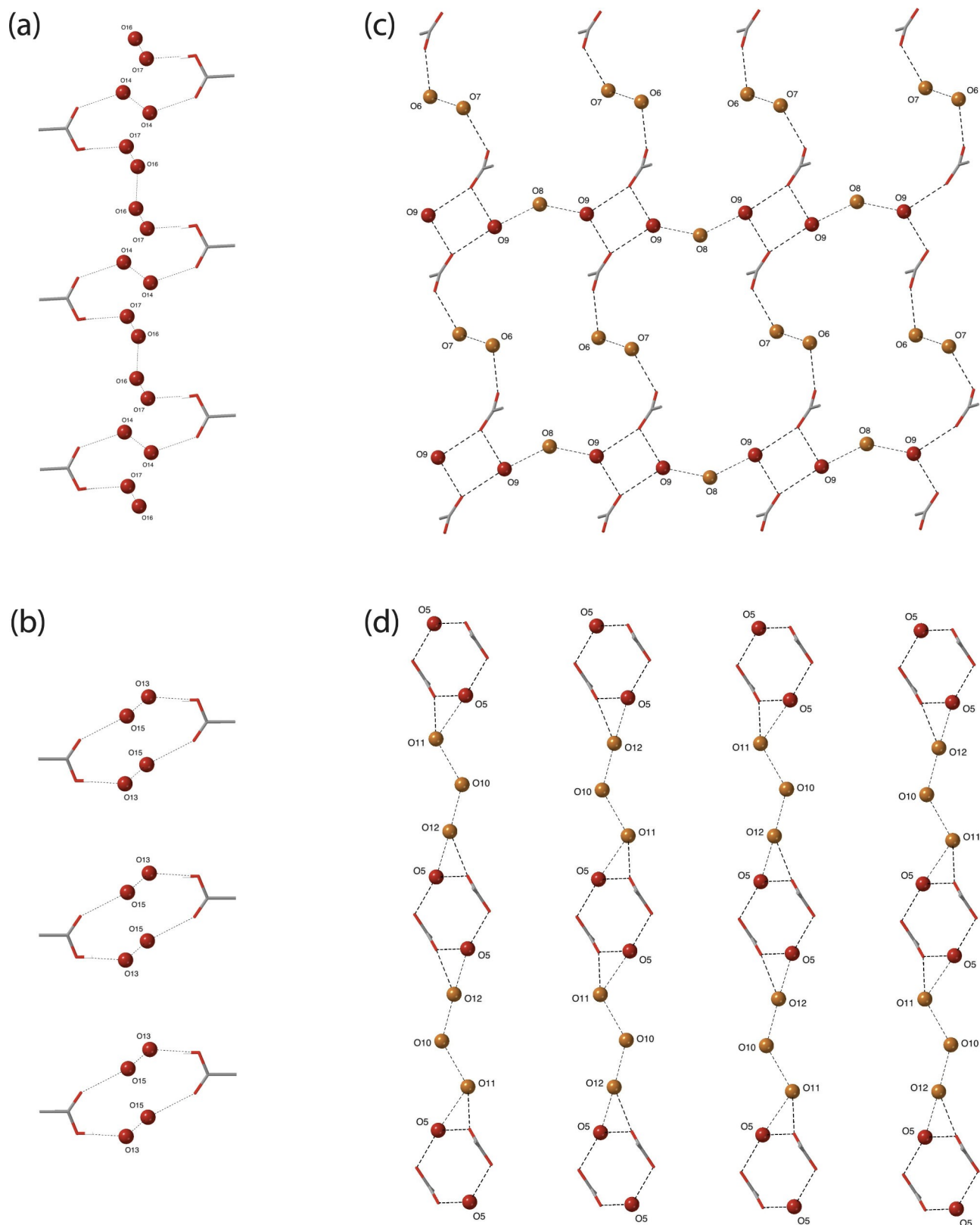


Fig. S9 Detailed views of the H-bonded 1D (a) and 0D (b), and 2D (c) and 1D (d) frameworks developed in **1** and **2**, respectively. The hydrogen bonding interactions involving crystallisation waters are drawn as dotted lines. Oxygen atoms of crystallisation waters are shown as red spheres, except those that have a structural disorder that appear in orange.

EPR spectra

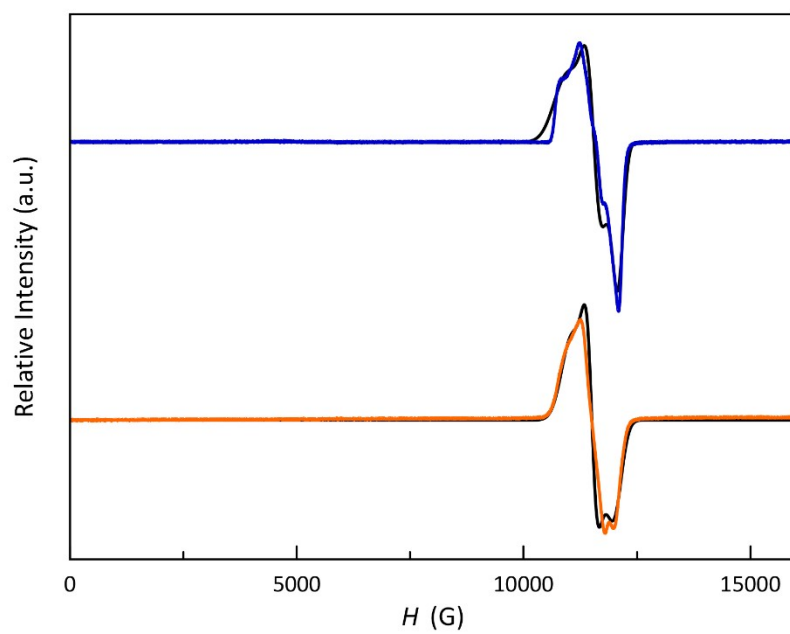


Fig. S10 Q-band EPR spectra of **1** (blue) and **2** (orange) at 4.0 K in the solid state. The black lines are the simulated spectra for a LS Co^{II} ion.

Static and dynamic magnetic properties

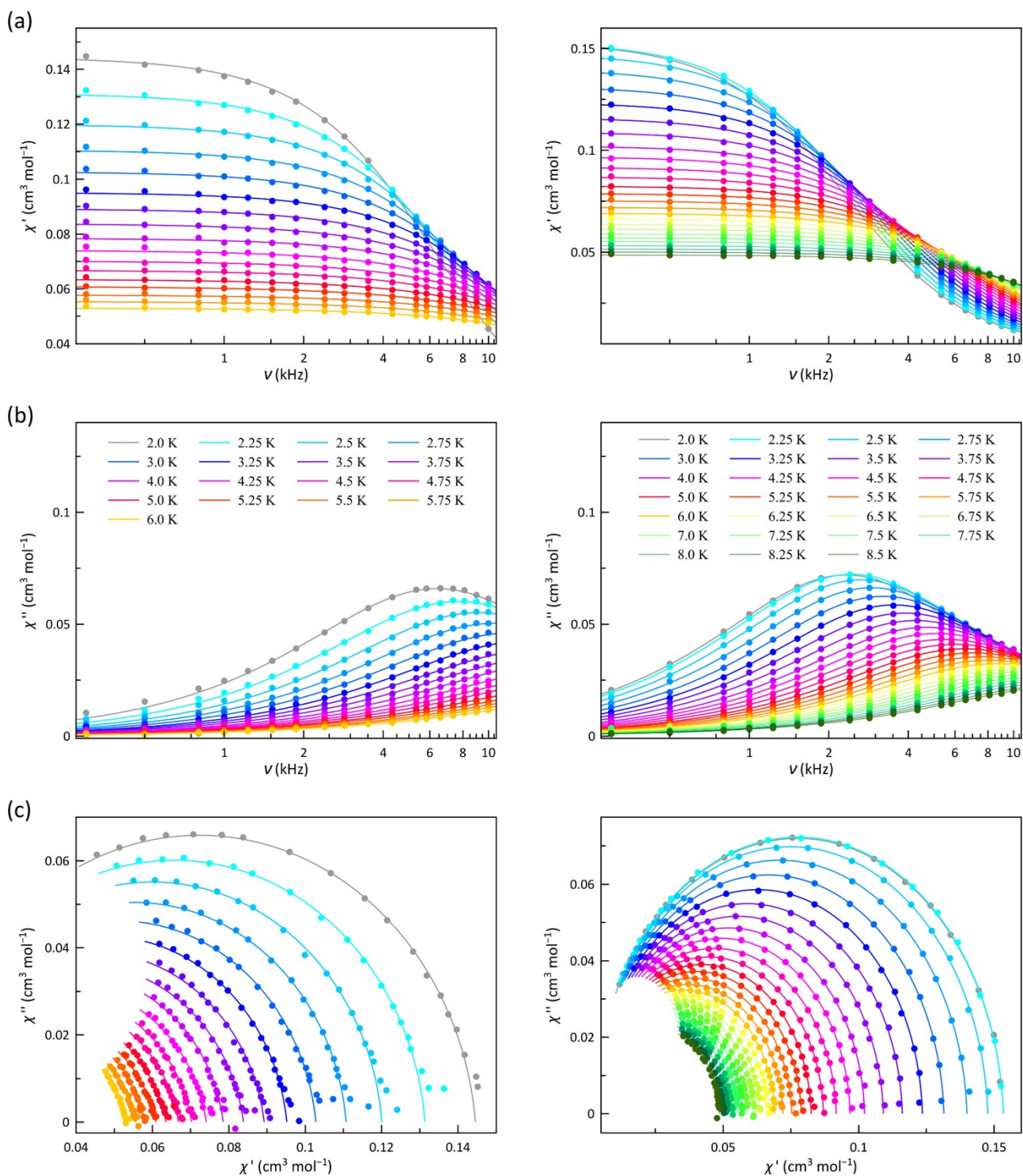


Fig. S11 Frequency dependence of χ_M' (a), χ_M'' (b), and the Argand plot (c) of **1** (left) and **2** (right) under a 2.5 kOe static and a ± 0.5 Oe oscillating magnetic fields in the temperature ranges 2.0–6.0 (**1**) and 2.0–8.5 K (**2**). The solid lines are the best-fit curves.

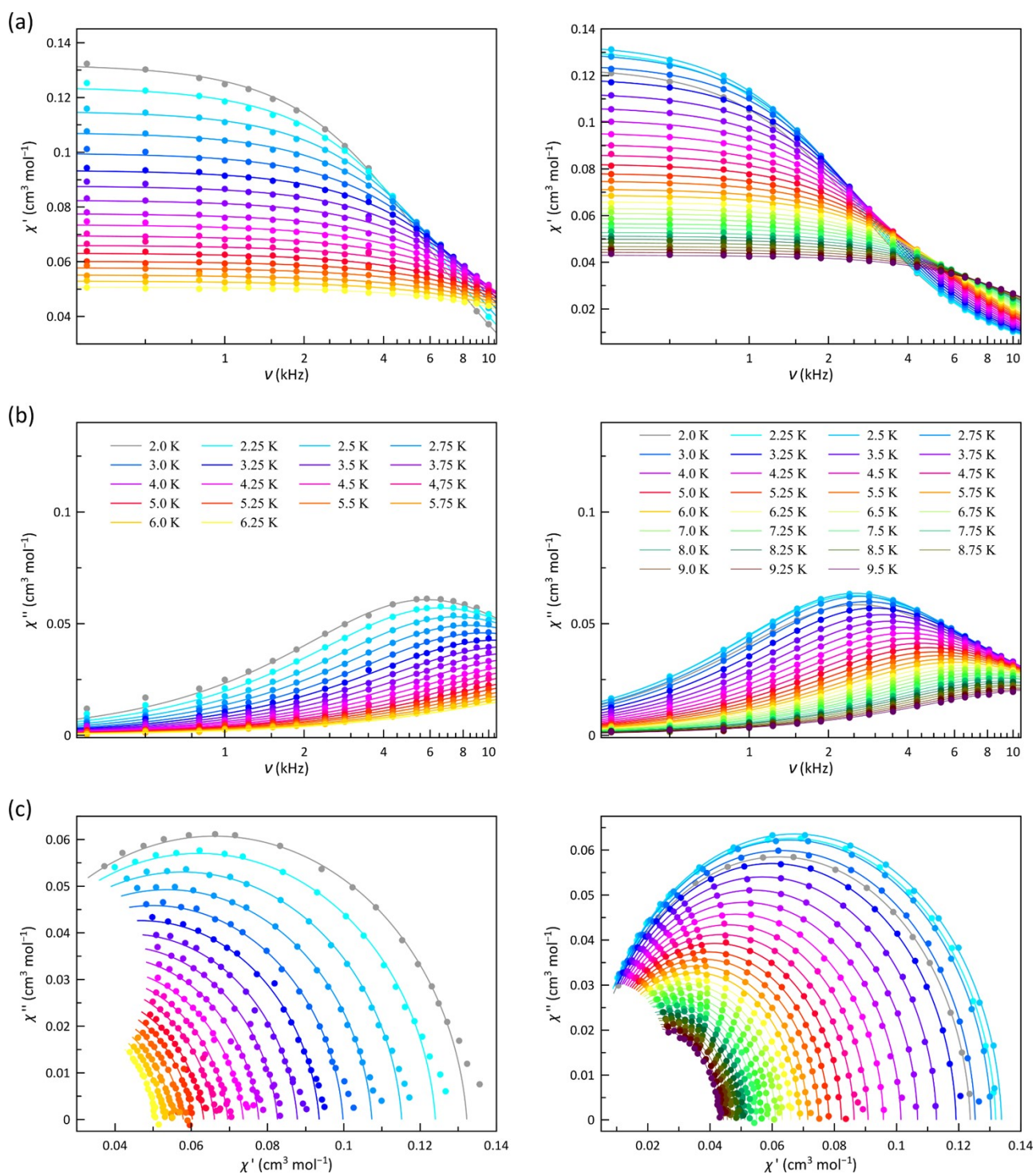


Fig. S12 Frequency dependence of χ'_M (a), χ''_M (b), and the Argand plot (c) of **1** (left) and **2** (right) under a 3.5 KOe static and a ± 0.5 Oe oscillating magnetic fields in the temperature ranges 2.0–6.25 (**1**) and 2.0–9.5 K (**2**). The solid lines are the best-fit curves.

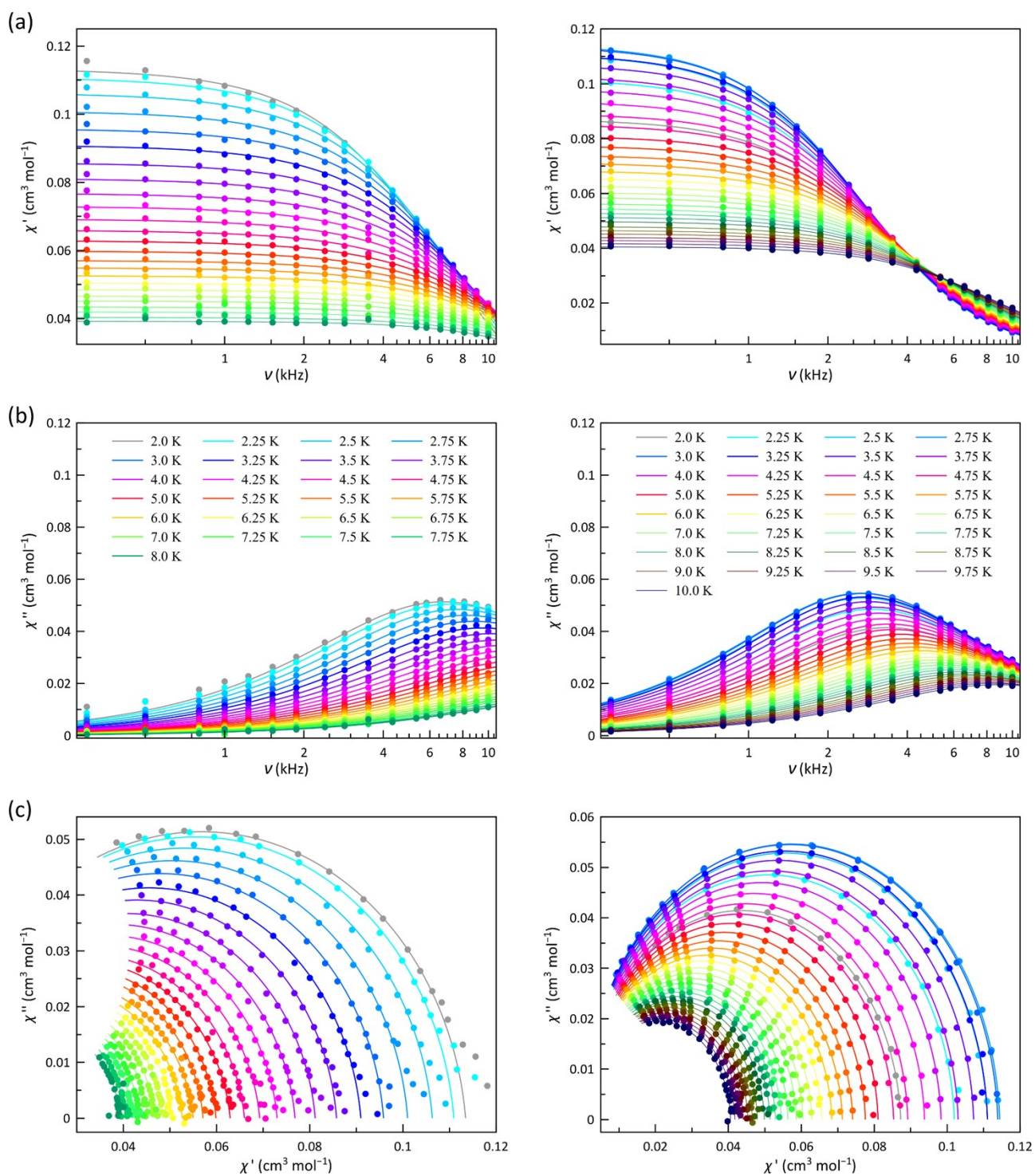


Fig. S13 Frequency dependence of χ_M' (a), χ_M'' (b), and the Argand plot (c) of **1** (left) and **2** (right) under a 5.0 KOe static and a ± 0.5 Oe oscillating magnetic fields in the temperature ranges 2.0–8.0 K (**1**) and 2.0–10 K (**2**). The solid lines are the best-fit curves.

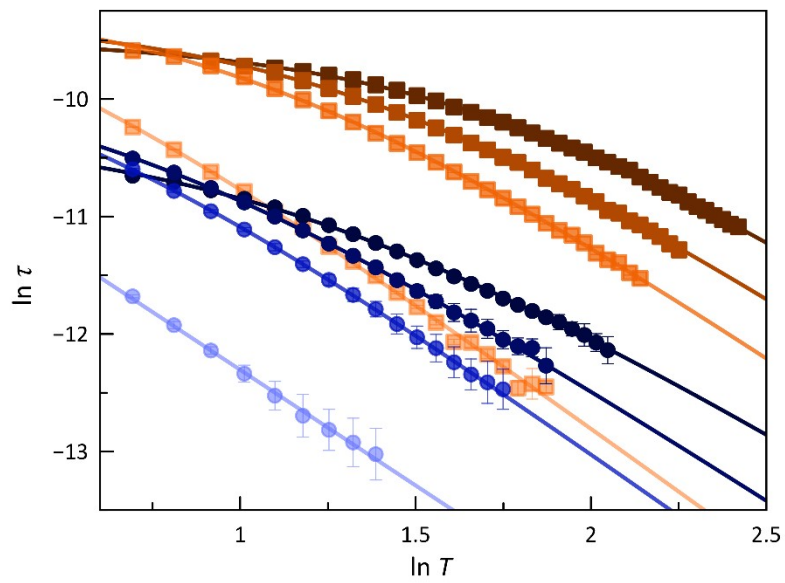


Fig. S14 $\ln \tau$ vs. $\ln T$ plots of **1** (●) and **2** (■) under applied *dc* magnetic fields of 1.0, 2.5, 3.5, and 5.0 kOe (from light to deep colours). The solid lines are the best-fit curves for a double Raman plus intra-Kramers (IK) relaxation mechanisms (see text). Vertical error bars denote the standard deviations.

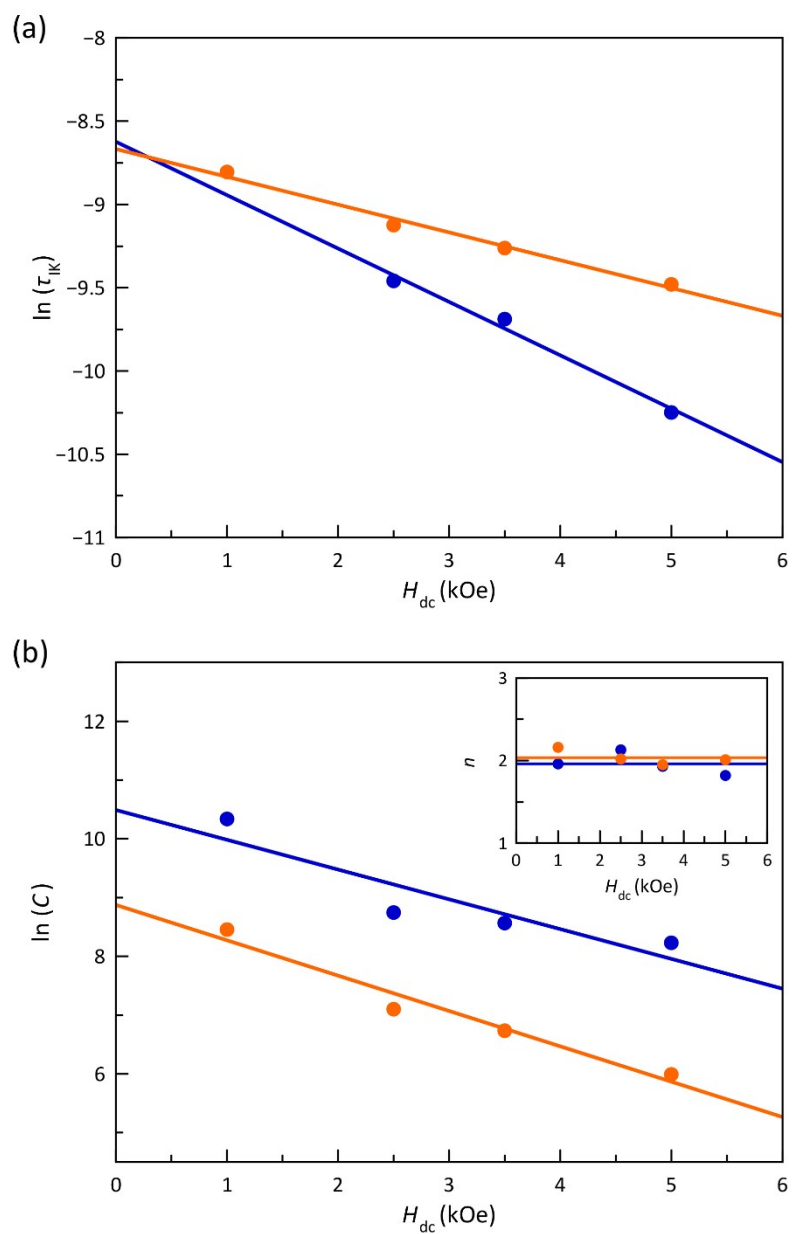


Fig. S15 Field dependence of the calculated values of τ_{IK} (a) and C (b) for a double Raman plus intra-Kramers (IK) relaxation mechanism in **1** (blue) and **2** (orange). The inset shows the field dependence of the calculated n values. The solid lines are the best-fit curves (see text).

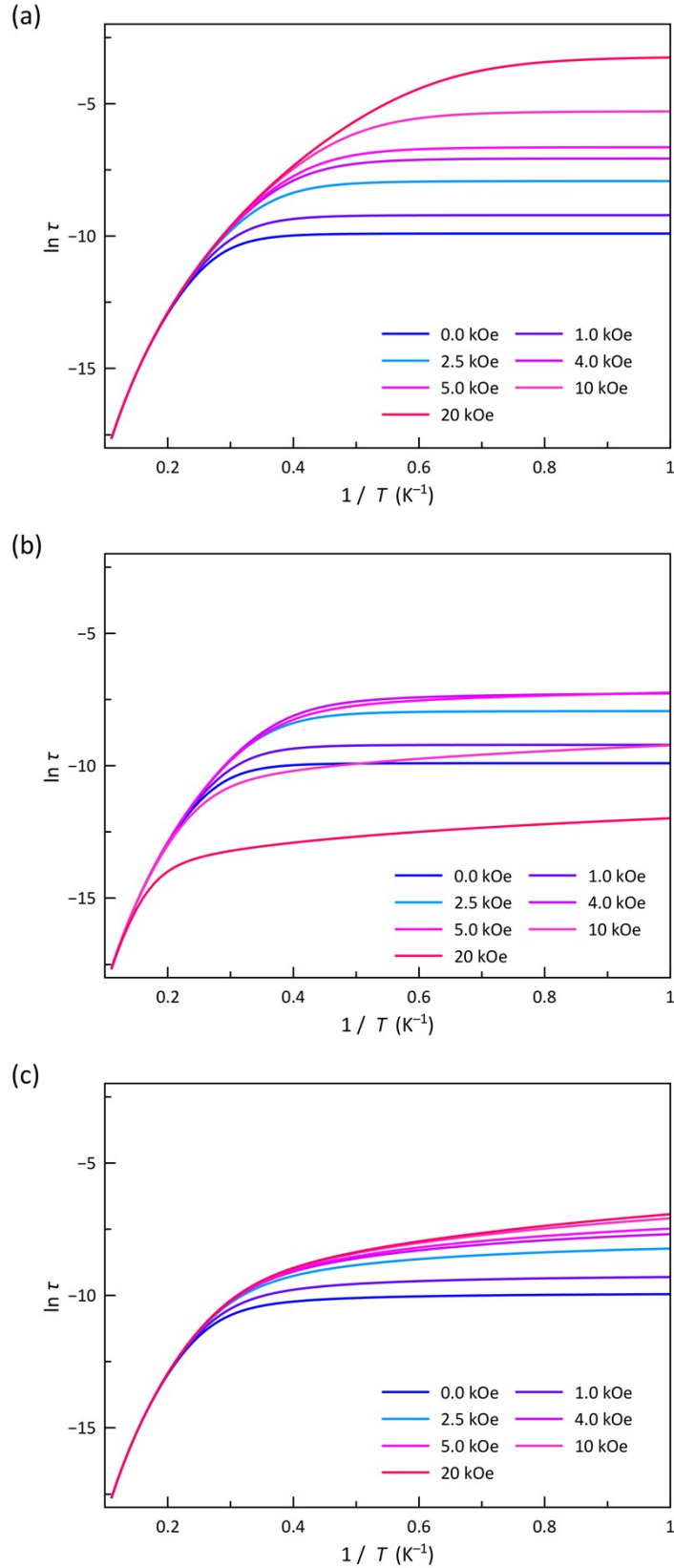


Fig. S16 Magnetic field dependence of the Arrhenius plots generated from a model considering IK, direct, and Raman mechanisms, the last one from optical and acoustic phonons [$\tau^{-1} = B_1/(1 + B_2H^2) + A_1H^4T + R_2T^2 + R_3T^9$]. In all simulations, $B_1 = 20000 \text{ s}^{-1}$, $B_2 = 1 \text{ kOe}^{-2}$, and $R_3 = 1 \text{ s}^{-1}\text{K}^{-9}$. (a) IK plus acoustic Raman: $A_1 = 0.0 \text{ s}^{-1}\text{kOe}^{-4}\text{K}^{-1}$ and $R_2 = 0.0 \text{ s}^{-1}\text{K}^{-2}$; (b) IK plus acoustic Raman plus direct: $A_1 = 1.0 \text{ s}^{-1}\text{kOe}^{-4}\text{K}^{-1}$ and $R_2 = 0.0 \text{ s}^{-1}\text{K}^{-2}$; and (c) IK plus acoustic Raman plus optical Raman: $A_1 = 0.0 \text{ s}^{-1}\text{kOe}^{-4}\text{K}^{-1}$ and $R_2 = 1000.0 \text{ s}^{-1}\text{K}^{-2}$.

Solution studies

Electronic absorption spectra were recorded on a Jasco UV/Vis/NIR V-670 spectrophotometer, whereas the emission spectra were recorded with a modular spectrofluorometer in the range $\lambda_{em} = 335\text{--}550$ nm with an excitation wavelength of $\lambda_{exc} = 295$ nm. The emission spectra of a 0.01 mM of **1** in DMSO/H₂O (80:20) solution were recorded at different pH values at 25 °C. Diluted aqueous solutions of HCl and NaOH were used to adjust the hydrogen ion concentration of the medium and the pH value was measured with a pH meter, previously calibrated with standardised buffer solutions at two pH values (pH 4.01 and 7.00). The computer program HypSpec⁷ was used to estimate the stability constants from spectroscopic data.

Cyclic voltammetry studies were performed using an AUTOLAB 204 scanning potentiostat operating at a scan rate of 200 mV s⁻¹. Cyclic voltammograms were recorded at room temperature using 0.1 M *n*-Bu₄NPF₆ as supporting electrolyte and 1.0 mM of **2** in DMF. The reference electrode was an AgCl/Ag, while a platinum disk (0.32 cm²) and a glassy carbon rod (76 mm) were used as working and auxiliary electrodes. All experiments were performed in standard electrochemical cells. The investigated potential was in the range from -2.0 to +1.0 V vs. AgCl/Ag. Ferrocene (Fc) was added at the end of the measurements as an internal standard. Formal potentials were defined as half-wave potentials, except for the irreversible reduction waves for which the anodic peak potentials were given instead. They were measured at a scan rate of 200 mV s⁻¹ and referred to the Fc⁺/Fc couple. The formal potential and the anodic to cathodic peaks separation of ferrocene under the same conditions were $E(\text{Fc}^+/\text{Fc}) = +0.42$ V vs. AgCl/Ag and $\Delta E_p(\text{Fc}^+/\text{Fc}) = 127$ mV (DMF, 0.1 M *n*-Bu₄NPF₆, 25 °C). The pH variable measurements were carried out by adding progressive amounts of aqueous 3.0 M HCl or *n*-Bu₄NOH solutions. For each recorded cyclic voltammogram, the electronic spectrum was registered in a Jasco UV/Vis/NIR V-670 spectrophotometer between 400 and 700 nm on an aliquot, later returned to the electrochemical cell.

⁷ Gans, P.; Sabatini, A.; Vacca, A. Investigation of equilibria in solution. Determination of equilibrium constants with the HYPERQUAD suite of programs. *Talanta* **1996**, *43*, 1739–1753.

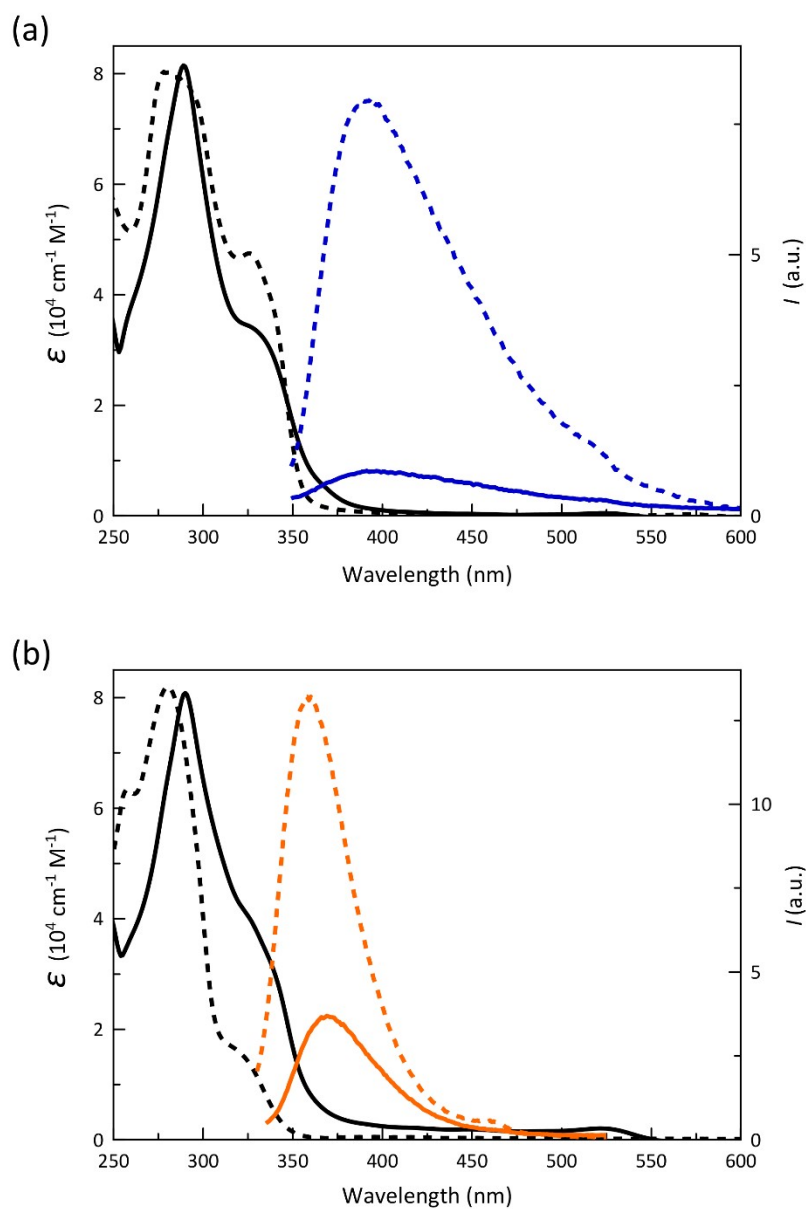


Fig. S17 (a) Electronic absorption (black) and emission (blue/orange) spectra ($\lambda_{\text{exc}} = 295 \text{ nm}$) of 0.01 mM solution of **1** at pH = 3 (a) and 8 (b) at room temperature, compared to those of 0.01 mM solutions of the corresponding protonated and deprotonated forms of the ligand, respectively (dashed lines). See text.

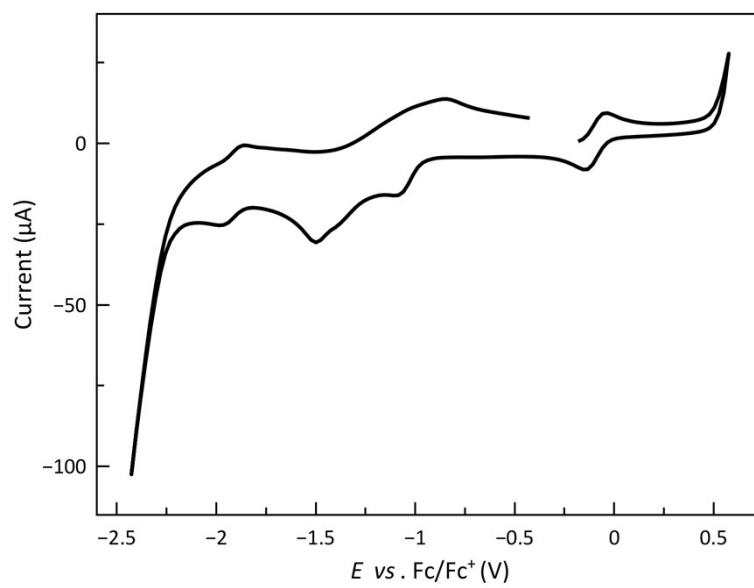


Fig. S18 Cyclic voltammograms of **2** in DMF [0.1 M *n*-Bu₄NPF₆] at 25 °C and 200 mV s⁻¹.

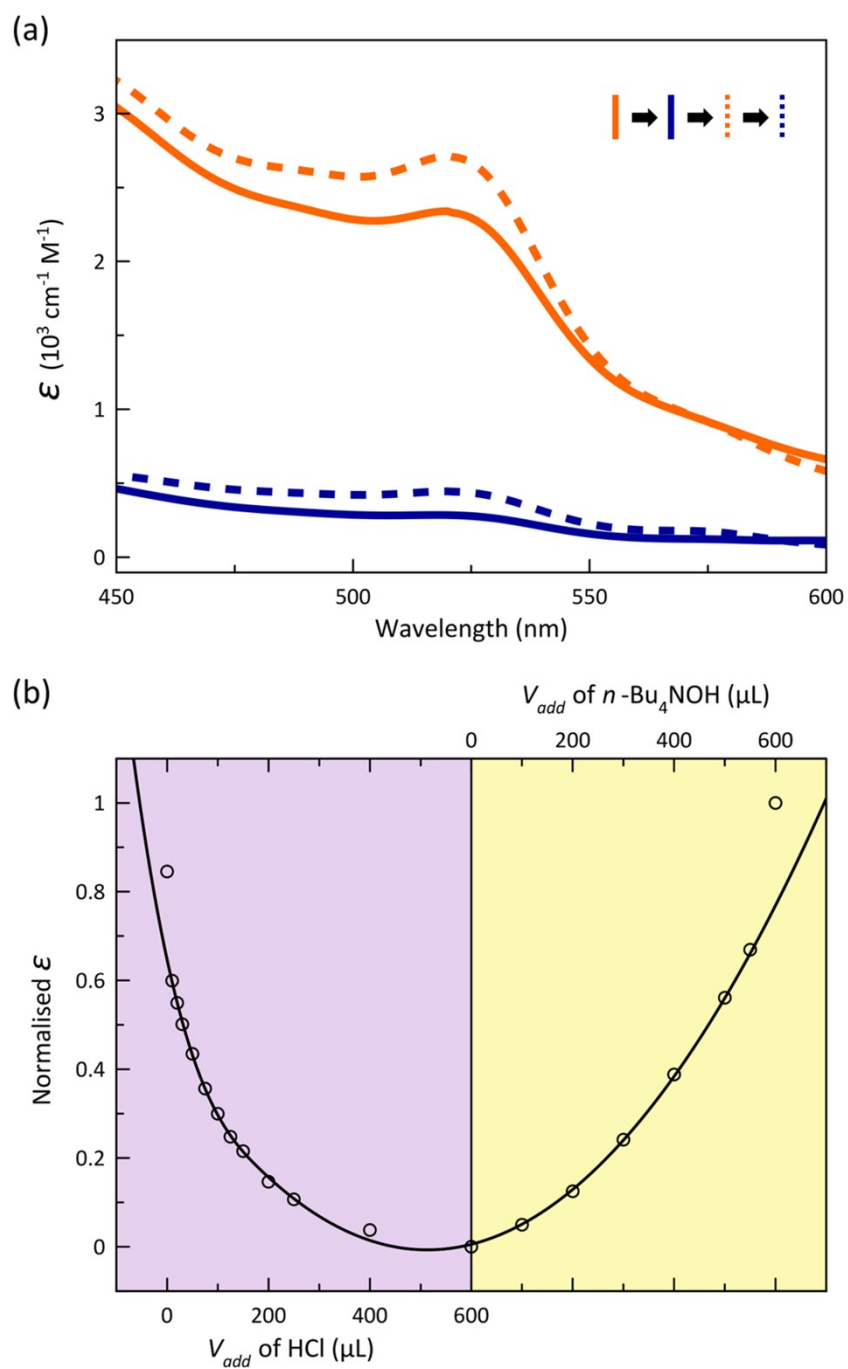


Fig. S19 (a) Electronic spectra of a solution of **1** in DMF [0.1 M $n\text{-Bu}_4\text{NPF}_6$] at 25 °C and 200 mV s^{-1} in acidic (blue) and basic media (orange) shown as solid lines. The restoration of the molar absorptivity after one cycle is represented as blue and orange dashed lines (see text). (b) Normalised Δp versus added volume of HCl (purple region) or $n\text{-Bu}_4\text{NOH}$ (yellow region). The solid black line is only an eye-guide (see text).